ITC 4/53
Information Technology and Control
Vol. 53 / No. 4/ 2024
pp. 1101-1118
DOI 10.5755/j01.itc.53.4.37642

Contour Detection by a Dark-Adaptation Model

Received 2024/06/14 | Accepted after revision 2024/09/24

HOW TO CITE: Zhou, W., Qiao, Y. (2024). Contour Detection by a Dark-Adaptation Model. *Information Technology and Control*, 53(4), 1101-1118. https://doi.org/10.5755/j01.itc.53.4.37642

Contour Detection by a Dark-Adaptation Model

Wei Zhou, Yakun Qiao

School of Information Engineering, Liuzhou City Vocational College, Liuzhou, Guangxi, China;
e-mails: zhouwei_lcvc@163.com; gxkjdx_qyk@163.com

Corresponding author: zhouwei_lcvc@163.com

The color contour detection model used for simulating the cone photoreceptor cell- lateral geniculate nucleus (LGN) – primary visual cortex (V1) visual pathway has achieved reliable results. In contrast, the rod photoreceptor cells employ a dark adaptive mechanism, which plays a key role in contour extraction in poorly lit environments. We employ this mechanism to propose a bionic model for contour detection. The proposed model divides the dark adaptation process into several stages and extracts the image information at each stage for subsequent integration. For evaluation, we applied the proposed dark adaptation model as the front-end processing method of the gray and color contour detection model, and performed experimental verification on the RuG, BSDS300/500, and NYUD databases. In comparison with a similar state-of-the-art model, the detection performance of the proposed model has several advantages; in particular, it extracts contour information more effectively in interior scenes lit with dim colors.

KEYWORDS: Computer Vision, Bionic Model; Contour Detection; Rod Cell; Dark Adaptation.

1. Introduction

The Contour is the most essential information regarding a target in a natural image. An effective contour detection method can extract the contour features of the target from complex interference information, which is conducive to improving the robustness of subsequent advanced visual tasks, such as target recognition [24] and image segmentation [32].

Contour detection is a highly challenging problem in the field of image processing. Unlike edge detection, contours are a part of the edge information, and hence, the results of edge detection cannot be used to define the contours. In digital images, edge detection finds and identifies points with significant changes in brightness, which usually includes texture edge information. In contrast, contour detection involves the extraction of target contours from digital images containing both targets and backgrounds, while ignoring the background effects, internal textures, and noise interference in the images. Common edge differential operators include Prewitt [37], Roberts [46], Sobel [11], and Laplace [33]. These operators are usually sensitive to noise, and their edge detection perfor-

mance in simple scenes is acceptable. However, their performance has been found to significantly reduce in images portraying more complicated scenes. In 1986, Canny [4] proposed a multi-level edge detection algorithm. However, indicating a surplus of noise when the Canny's algorithm is used. To improve the accuracy of the target contour, researchers have proposed the use of several traditional contour detection methods based on edge detection. These include statistical approaches, phase congruency and local energy, grouping pixels into contours according to Gestalt principles, and contour detection in the scale space [25].

Owing to the advancement of intelligent computing over the past few years, convolutional neural networks (CNN) have been widely used in the field of computer vision. CNNs are being applied to numerous image processing tasks, such as image classification [37], which has significantly improved the accuracy of these tasks as compared to the case using traditional methods. Presently, numerous CNN-based contour detection methods have been proposed. These methods employ the VGG or RESNET as the encoding networks, use their own decoding networks, train the original images and prescribed contours into the network, and adjust the parameters of the convolution kernel in the network using the loss function, such that the contour of the output of the network corresponds to the specified contour. For example, PMI [10], COB [20], and CED [34] have achieved good experimental results. However, these methods use supervised learning, the performance of which relies heavily on the availability of a large amount of data. Furthermore, the learning process is also highly time-consuming. Furthermore, it cannot flexibly and rapidly process specific images, and the calculation cost is generally very high.

In the recent years, research on bionic contour detection has attracted significant attention. Physiological studies have shown that target contour information is mainly extracted from the first visual pathway of biological vision (retina-LGN-V1). Inspired by this mechanism, numerous biomimetic contour detection models have been proposed, which are mainly divided into gray and color image models. In the retina, these two models employ different physiological mechanisms. Models for grayscale information processing mainly mimic the physiological mechanism of the ganglion cell layer in the retina, while models for color information processing mainly simulate the photoreceptors (cones) in the retina [14, 29].

Among the bionic studies on contour detection in grayscale, the bionic model of the single primary visual cortex is the most widely used and yields good results. In 2003, Grigorescu et al. [8] first proposed a contour detection method based on a non-classical receptive field by utilizing isotropic inhibition (ISO) and anisotropic inhibition (ANI). However, some regions that are not classical receptive fields exhibit facilitation rather than inhibition during the information response process. To this end, Zeng et al. [44] proposed a butterfly-shaped inhibition model, using a unilateral regional inhibition algorithm to simulate the mechanism around the cell center with high accuracy. In the same year, they improvised this model [43] and proposed a two-sided + two-ended (adaptive) suppression algorithm, which effectively simulated the effect of the non-classical receptive field on the center and improved the accuracy of contour detection. However, all these algorithms perform contour extraction at a single scale, which results in the loss of information. Therefore, the multi-scale fusion method [36] was proposed, which effectively improved the accuracy of contour detection. The proposed model was used all around in front of the local information of inhibition and did not consider the direction of the cell response. Thus, Xiao and Cai [38] introduced a novel angle as a measure of the neighboring neuron response in the optimal direction and the difference in the optimal neuron direction angle in the response center, to determine the mechanism of the action of neurons to the center of. In this method, the separation of the facilitation and inhibition regions can be avoided, and the corner and t-shape contours can be effectively enhanced. Furthermore, Cao et al. [5] applied the center-periphery mechanism and proposed a method to extract the local center-periphery contrast information from natural images using the normalized Gaussian difference function and the sigmoid activation function. In comparison with the traditional algorithm, the computational complexity of this method is low, computational speed is faster, and performance is superior. Although the bionic model employs peripheral modulation to emphasize the directional modulation characteristics of all the peripheral information, it is difficult to extract the contour defined by other clues, although several models have been proposed to improve the contour detection ability using the multi-

scale strategy [12]. To employ more image information for contour detection, Yang et al. [42] suggested that a combination of multiple clues could be used to further enhance the suppression of texture information. By introducing the direction, brightness, and contrast, the weight of the suppressed items could be adjusted to further improve the contour detection effect.

To simulate the retina (ganglion cells), Wei at el. [35] proposed an image preprocessing model for the ganglion cells layer and the difference of Gaussians (DoG) function is used to calculate the equivalent values of the red, green, and blue levels in the image to dynamically adjusted the size of the sensory field. To simulate the LGN layer, Azzopardi and Petkov [2] proposed a computational model for contour detection in the combined receptive field (CORF), considering the arrangement of On and Off receptive fields in the LGN layer. Parameters such as polarity, scale, radius, and polar angle were introduced, which reflect the informational characteristics of the receptive field. In 2014, the CORF model was improved, and a push-pull CORF model was proposed. The response mode (excitation or suppression) was determined according to the polarity preference of CORF (On or Off), which had a good effect on noise suppression [3]. With regard to the retina (ganglion cells) – LGN – primary visual cortex, Spratling [28] considered opponent properties of the On and Off receptive fields of the LGN layer, and introduced a sparse coding algorithm in the V1 layer model to establish the contour detection model of the LGN to the V1 layer visual pathway. Inspired by the physiological mechanism of the x-y visual pathway, Lin et al. [18] introduced the summative characteristics of the field space of Y cells into the visual processing mechanism of the V1 layer and proposed a linear and nonlinear suppression contour detection model based on the x-y visual pathway by combining the various scale image information of X and Y cells into a single inhibition term. Melotti et al. [22] proposed a contour operator that combines the push-pull and surround suppression. The proposed model is a combination of the receptive field (CORF) model and the push-pull inhibition, extended with surround suppression, which inhibits a part of the texture to a certain extent.

In comparison to grayscale, a color image provides more detailed features. Results indicate that the contour detection method based on color features, which mainly adopts the retinal (cone cell) -LGN-V1 visual pathway, is superior to that based on gray features. Zhang et al. [45] proposed a color information descriptor based on the color antagonism mechanism, which effectively improved the performance of tasks such as target recognition and boundary detection. Other similar methods employ the information processing method of color antagonism to improve the algorithm performance. For example, Martin et al. [21] calculated the local image gradients in red-green and blue-yellow opponent channels to detect color boundaries. However, these methods, which are based on color opponents, only detect the boundary contour based on the color, whereas that of brightness is not addressed. Therefore, to extract the boundary information from a color image (the natural image usually contains both brightness and color boundaries), it is often necessary to detect the brightness features. Yang et al. [40] presented a CO model that uses the retinal photoreceptor cone – LGN – V1 visual pathway, where the visual cone cells in the retina use a Gaussian function to receive information from the color information extraction. Furthermore, for the LGN and V1 layer, the model uses the theory of color single antagonism and dual antagonism to extract the target contours in the image. For more accurate contour extraction from color images, Yang proposed the SCO [41] model, which is based on the CO model, and suggested a sparse coding mechanism for the extra texture in the CO model to reduce texture doping in the contour regions.

In summary, the contour extraction model for the grayscale image is mainly based on the single simulation of V1, retinal ganglion cells, LGN, and retinal ganglion cells-LGN-V1. The color model mainly simulates the retinal cone photoreceptor cells-LGN-V1. Although both the grayscale and color bionic contour detection models involve simulation of the retina, the results obtained are not comprehensive. They are mainly applied to retinal ganglion cells (grayscale model) and retinal photoreceptor cones (color model) and are not effective in the case of other types of photoreceptor-rod cells. For photoreceptors, the visual acuity of the retina decreases in the presence of light (light adaptation) and increases in darkness (dark adaptation), thereby maintaining an appropriate visual acuity over a wide range of illuminance. The visual adaptation system adapts to the current environment

by coordinating the pupil, the rod and cone system, photochemical reactions, and neural mechanisms [7]. Shlaer et al. [27] argued that the visual acuity of human eyes is related to the brightness of the environment. In a dim environment, human eyes become extremely sensitive, which gives them the ability to detect subtle changes in brightness at the cost of the ability to recognize detailed features and colors of objects. In an environment lit with sufficient bright light, human eyes have relatively good color vision and strong visual acuity. However, the sensitivity to the change of brightness becomes lower in this scenario, and therefore, only a significant change in brightness can be detected by the human eye. Hecht et al. [9] pointed out that light and dark adaptation simply indicates habituation to lower or higher levels of ambient lighting. Although we may not be clearly aware of this mechanism, our visual performance changes dramatically based on the situation. Dark adaptation occurs because of the increased synthesis of rhodopsin in rod cells. Drawing inspiration from these mechanisms, we propose a simulation model of the dark adaptation process by investigating the dark adaptation mechanism in the retina. We simulate the adaptation process at different stages for various types of target information and subsequently integrate the results to obtain a highly comprehensive information, extract the relatively complete details. Finally, we use DA to refer to the dark adaptation model, and the terms DAG and DAC to refer to the gray and color dark adaptation contour detection models, respectively.

The remainder of this article is organized as follows: Section 2 describes the proposed DA model in detail. In Section 3, the grayscale and color dark adaptive contour detection models are introduced. Section 4 evaluates the contour extraction performance of the proposed model in grayscale and color images through multiple data sets. Section 5 describes the experimental results of combining the model without non-maximum suppression with deep learning contour detection algorithms in this paper. The discussion and conclusions are provided in Section 6.

2. Dark Adaptation Model

In this study, the dark adaptation mechanism on the retina was simulated, and the theoretical-maximum-luminance image of the corresponding stage is obtained using the formulas (1) and (2). Subsequently, this image is compared with the original image, and the pixel points that meet the requirements are screened out to generate the actual-maximum-luminance image. The framework of the DA model is illustrated in Figure 1. For a better understanding, follow-up DA models were illustrated in four stages. The process of dark adaptation refers to the gradual increase in visual sensitivity when entering a dark area from strong light or when lighting suddenly stops, allowing for the resolution of surrounding objects. This process can be divided into four stages.

Figure 1

Dark adaptation model flow chart. The original brightness image was compared with the theoretical-maximum-luminance image of each stage, and the actual-maximum-luminance image of each stage was obtained

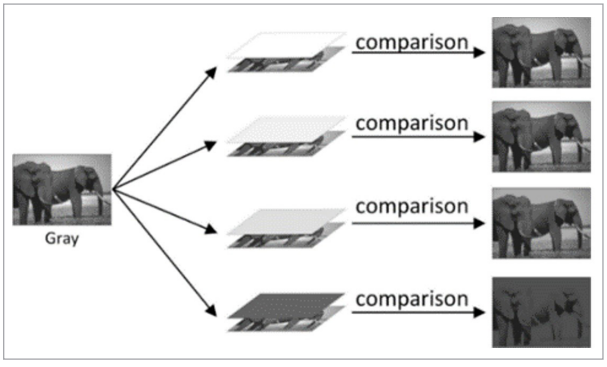

Primary adaptation period: In a bright environment, most of the rhodopsin (a chemical substance sensitive to weak light) in the rod cells is broken down, so when entering darkness, the rod cells have a weaker response to weak light. As time goes by, the synthesis of rhodopsin begins and the rod cells gradually recover their function.

Intermediate adaptation period: With the continuous synthesis of rhodopsin, the sensitivity of rod cells to weak light gradually increases. The pupils are further dilated to increase the amount of light entering the eyes, thereby further enhancing visual sensitivity.

Advanced adaptation period: At this point, the rod cells have fully recovered and are in their optimal working state, able to produce sufficient photoreceptor. The visual nerve center has also undergone corresponding adjustments to adapt to low light conditions.

Long term adaptation period: Rod cells will continue to play a role in the dark environment, maintaining an adaptive state of vision. The synthesis of rhodopsin will also continue, increasing the sensitivity of the eyes to low light. This process can last for several hours or even longer.

We simulate the adaptation process of the brightness and consider the brightness of the original image as the end of the adaptation process. Because the dark adaptation process occurs when going from a well-lit area to a dark area, we have $V_t \in (0,1)$. In [13], a function was used to simulate the change in the light sensitivity of the adaptive state of the visual cell. Therefore, we set the calculation function of the theoretical-maximum-luminance value at the current adaptation time as follows:

$$A_t = 1 - e^{-\frac{t}{\tau}}. \tag{1}$$

In rod cells, the photosensitivity of the nerve can be adjusted within 200 ms, $t \in (1, 200)$, and the adaptation time of the rod cells is given by $\tau = 150$ ms [26]. To filter out the optimal theoretical-maximum-luminance during the adaptation process, we divide the time t into n equal parts and use the brightness level corresponding to the time as the theoretical-maximum-luminance at that moment. Next, we set the brightness value of all the pixels in the image to the theoretical-maximum-luminance, and refer to the current image as the theoretical-maximum-luminance image V_t. The brightness adaptation time of different pixels varies significantly; for example, when a pixel reaches the brightness level of the original image before the adaptation process is completed ($t \neq 200$), the pixel is considered to have completed the brightness adaptation (pixel complete adaptation), its brightness value no longer changes, and the unfinished pixels continue with the remainder of the adaptation process. We compare the obtained theoretical-maximum-luminance image with the original brightness image V to obtain the actual-maximum-luminance at the current moment:

$$Va_t(x,y) = \begin{cases} V(x,y) & V(x,y) \le V_t(x,y) \\ V_t(x,y) & V(x,y) > V_t(x,y) \end{cases}. \tag{2}$$

In Figure 2, four stages are presented as examples to illustrate the detailed changes of a pixel in a 5 × 5 area

Figure 2

Detailed process of brightness changes in dark adaptation. In each stage, the theoretical-maximum-luminance image is compared with the original brightness image to select the points whose brightness is less than the theoretical-maximum-luminance (if the comparison is √, the pixel is kept as the actual maximum value of the current stage; if it is , it is not handled), Finally, the unprocessed pixels and the pixels retained after the comparison are combined to form the actual-maximum-luminance image at the current stage

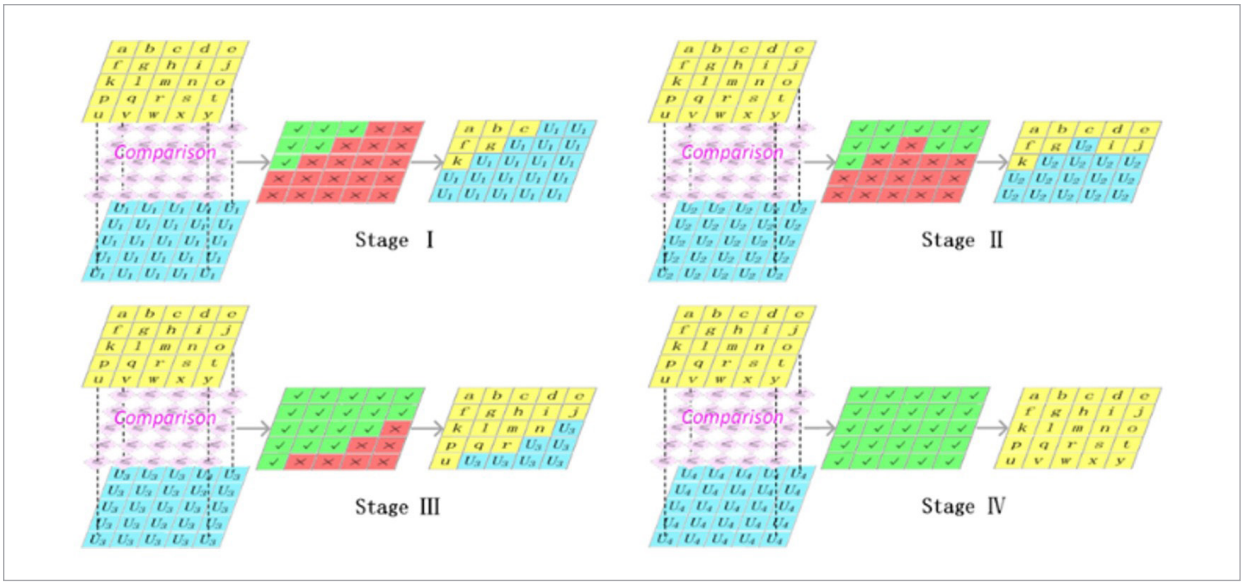

in an image under different theoretical-maximum-luminance during the adaptation process. The number of pixels that reach the actual-maximum-luminance at different adaptation moments is different. When all the image pixels reach the actual-maximum-luminance, the adaptation process is considered to be complete.

As mentioned above, the number of restored brightness points in the image at each moment is different, as the information is not the same at every moment. Thus, we perform a weighted fusion of the images at different adaptation moments, using the ratio of the number of pixels fully adapted to the total number of pixels at the current moment as the weight:

$$\omega_t = \frac{j}{N} \tag{3}$$

$$I(x,y) = \sum_{t=1}^{n} \omega_t \cdot I_t(x,y), \tag{4}$$

where j represents the number of pixels that have completed adaptation at the current moment (excluding the pixels that completed adaptation at the previous moment), and $I(x,y)$ is the image after adaptation.

Figure 3
Fusion weight calculation

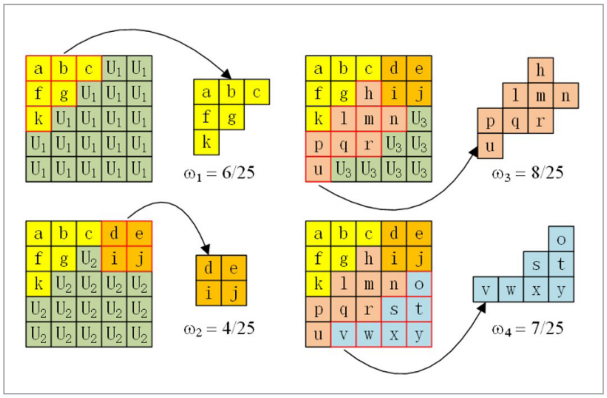

3. Contour Detection Model

The contour detection model comprises two components: the color information response (Section 3.1), which mainly performs color processing of the image. In the first component, the input RGB image is converted to a HSV color space (V), than changing the brightness for many times, the theoretical-maximum- luminance image is obtained, and compared with the original brightness image to get the actual-maximum- luminance image, following which a dynamic adaptation process is generated, and subsequently, RGB color space is transformed for each image, and the transformed image is fused by linear weighting. The other component of the model constitutes the grayscale information response provided by the rod cells (Section 3.2): here, the image is visually processed mainly in grayscale, and the dark adaption process is similar to the process of color information response. Finally, the grayscale images obtained from each stage are linearly weighted and fused.

3.1. Color Information Response

This study simulates the dark adaptation process of vision, where the color information response first transfers the input RGB image to the HSV color space as follows:

$$H = \begin{cases} 0^\circ & ,\Delta = 0 \\ 60^\circ \times \left(\frac{G'-B'}{\Delta} + 0\right) & ,C_{max} = R' \\ 60^\circ \times \left(\frac{B'-R'}{\Delta} + 2\right) & ,C_{max} = G' \\ 60^\circ \times \left(\frac{R'-G'}{\Delta} + 4\right) & ,C_{max} = B' \end{cases} \tag{5}$$

$$S = \begin{cases} 0 & C_{max} = 0 \\ \frac{\Delta}{C_{max}} & C_{max} \neq 0 \end{cases} \tag{6}$$

$$V = C_{max}, \tag{7}$$

where R'=R/255; G′=G/; B′=B/255, C_{max} and C_{min} represent the maximum value of each point in the RGB channel, C_{max} =max(R', G', B'), C_{min} = min(R', G', B'). Δ = C_{max}–C_{min} represents the difference between the maximum and minimum at each point.

After the brightness V is processed by the DA model, the actual-maximum-luminance images of n stages are transferred back to the RGB color space one by one, and n color images of different adaptive moments are obtained as follows:

$$C = Va_t \times S,\ X = C \times (1 - |(H/60^\circ) mod\ 2 - 1|),\ m = Va_t - C. \tag{8}$$

Figure 4
DAC model flow chart. After the DA model, images of each stage are transferred back to the RGB color space for weighted fusion

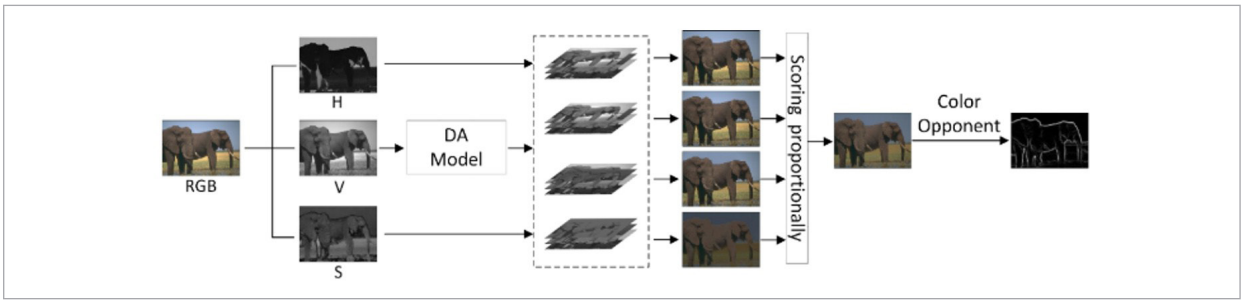

$$(R_t', G_t', B_t') = \begin{cases} (C, X, 0), & 0^\circ \le H < \pi/3 \\ (X, C, 0), & \pi/3 \le H < 2\pi/3 \\ (0, C, X), & 2\pi/3 \le H < \pi \\ (0, X, C), & \pi \le H < 4\pi/3\ ' \\ (X, 0, C), & 4\pi/3 \le H < 5\pi/3^\circ \\ (C, 0, X), & 5\pi/3 \le H < 2\pi^\circ \end{cases} \quad (9)$$

$$I_t = (R_t, G_t, B_t) = (R_t' + m) \times 255, (G_t' + m) \times 255, (B_t' + m) \times 255. \quad (10)$$

Finally, the target contour $Re_{color}(x, y)$ in the output image is extracted using the color opponent principle [7], as depicted in Figure 4.

3.2. Grayscale Information Response

The method for the processing grayscale image information is similar to that used in the case of color images. Equations (1)-(2) are used to adapt the grayscale image, and linear weighted fusion Equations (3)-(4) are used to obtain the gray information response output of the retina.

Finally, the Gabor function model [6] proposed by Daugman and sparse coding (SP) [41] was used to extract the target contour in the output image in response to the grayscale information of the retina, as depicted in Figure 5.

Figure 5
DAG model flow chart. After the DA model, images of each stage were directly weighted and fused

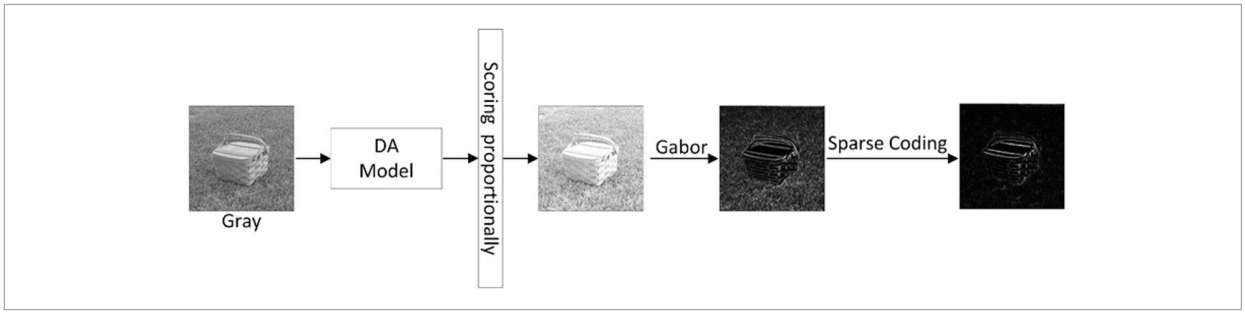

4. Experiment and Analysis

We perform non-maximum suppression on the entire output contour [8]. Subsequently, we evaluate the performance of our model on the RuG, Berkeley segmentation (BSDS300 / 500), and NYUD datasets [15] using the standard F-measure evaluation method [41]. We set the tolerance parameter maxDist to 0.0075 in all benchmark test, which represents the error tolerance of the contour.

$$F = \frac{2PR}{P + R} \quad (11)$$

$$P = \frac{TP}{TP + FP} \quad (12)$$

$$R = \frac{TP}{TP+FN}, \quad (13)$$

where TP represents the number of contour pixels that are correctly detected, *FP* represents the number of contour pixels that are incorrectly detected, *FN* represents the number of contour pixels that are missed; *P* represents precision, and *R* represents recall rate, *F* is the harmonic average of the both, which represents the similarity between the detected contour and the ground truth. ODS, OIS, and AP evaluated the performance of edge detection algorithms from different perspectives. ODS focuses on the average performance of the algorithm on the entire dataset, OIS focuses on the optimal performance of the algorithm on a single image, and AP provides an evaluation of the average performance of the algorithm over the entire recall range. These three indicators complement each other and together constitute a comprehensive evaluation of algorithm performance. Generally, the *F-measure* evaluation method corresponds to three standard performance indicators: ODS (the optimal threshold for the entire data set), OIS (the optimal threshold for each image), and AP (average accuracy).

4.1. Grayscale Model Performance Analysis

To test the effectiveness of the algorithm on grayscale images, we applied the DA model to the grayscale dataset and evaluated the performance of the algorithm from multiple perspectives. In this experiment, we set the receptive field size σ =6 the direction *ntheat*=8, spatial sparseness coding window size *ws*=5. As we can see that the DAG model superior to the other bionic contour extraction models on the RuG dataset.

To test the effectiveness of the algorithm on grayscale images, we applied the DA model to the grayscale dataset and evaluated the performance of the algorithm from multiple perspectives. In this experiment, we set the receptive field size σ=6 the direction *ntheat*=8, spatial sparseness coding window size *ws*=5. As we can see that the DAG model superior to the other bionic contour extraction models on the RuG dataset.

The proposed model has very low computational cost because its building blocks are simple simple convolution and mathematical operations. With this in mind, we report the average computational time of some algorithms for RUG in Table 1; Although the MATLAB implementation of DAG is slow, it outperforms nearly every method considered. We only used a single CPU core for computation and o mitted the computational time of the post-processing actions of NMS and hysteresis thresholding.

Table 1
Average computational time (s) of eight-edge detection models on RUG in the MATLAB framework with Intel(R) Core (TM) i5-9300H CPU @ 2.40GHz

Model	Time(s)
ISO [37]	0.22
Gabor + SP [41, 6]	0.34
CORF [5]	1.62
CORF+PP [5]	2.25
LI [43]	10.28
MCI [43]	23.06
DAG	0.66

In Figure 6, we show the qualitative experimental results of the DAG model with the RuG dataset. In the figure, we select the results of the improved optimal algorithm for qualitative comparison such as use CORF+PP instead of CORF.

4.2. Color Model Performance Analysis

When visual information from the environment enters the human brain, the information is first processed by the retina. An important physiological mechanism in this process is visual adaptation, from which various target information from different stages can be obtained. In this study, the number of stages of the process that we must adapt to are discussed, and the different data concentration curves of ODS, OIS, and AP are plotted and depicted. The maximum of each curve is marked, in the work the number of optimal stages is selected based on the maximum ODS (for NYUD, we use the RGB image screening test results datasets), as shown in Figure 7.

Figure 6

Binary contour images of six images from the RuG dataset. From top to bottom: the input image, corresponding ground truth, ISO [37], Gabor + SP [6, 41], CORF+PP [5], MCI [43], and DAG model. The values in the upper-right corner denote the P-scores

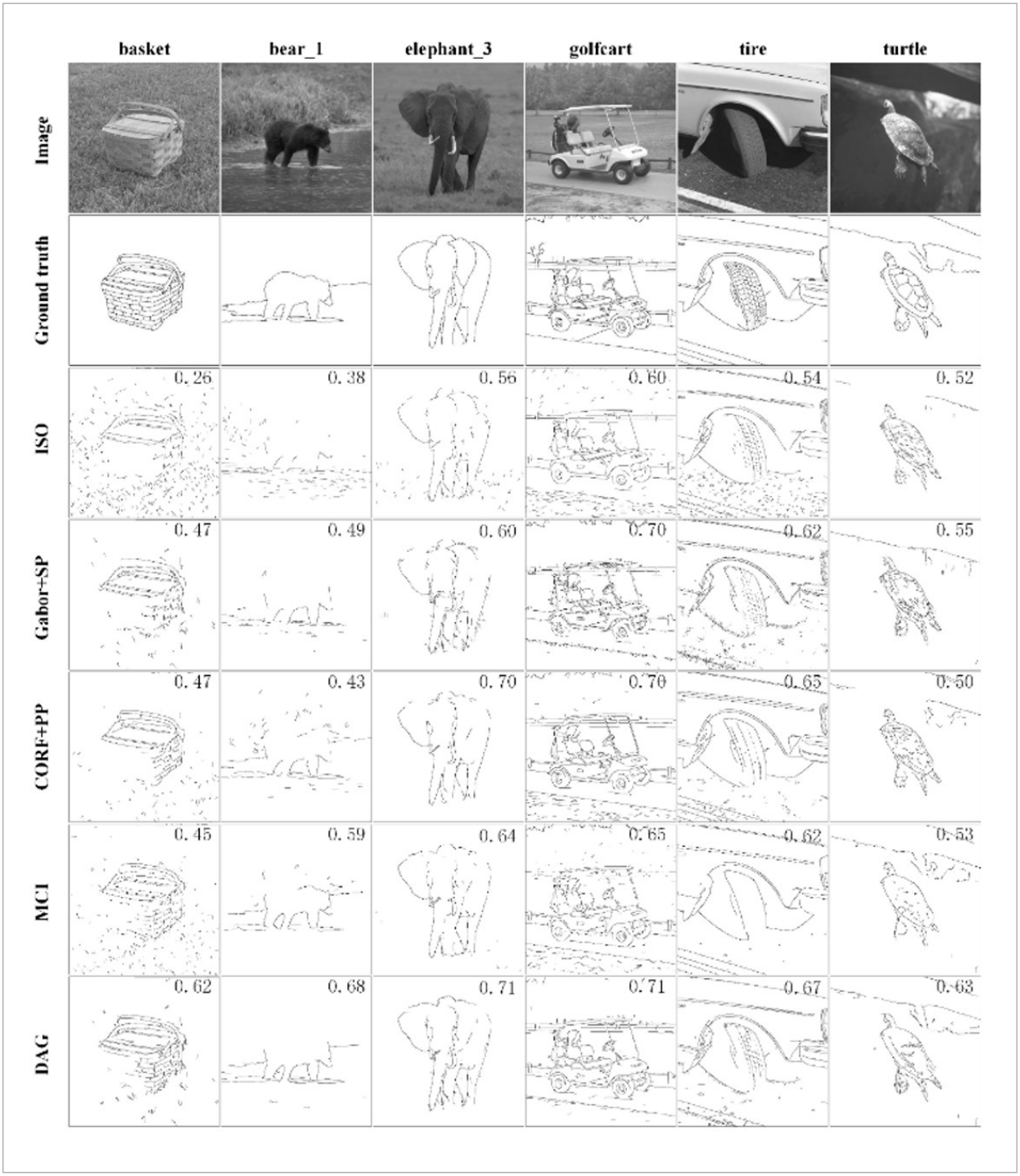

Figure 7
Data indicator curves of datasets (a) BSDS300 (b) BSDS500, and (c) NYUD (RGB)

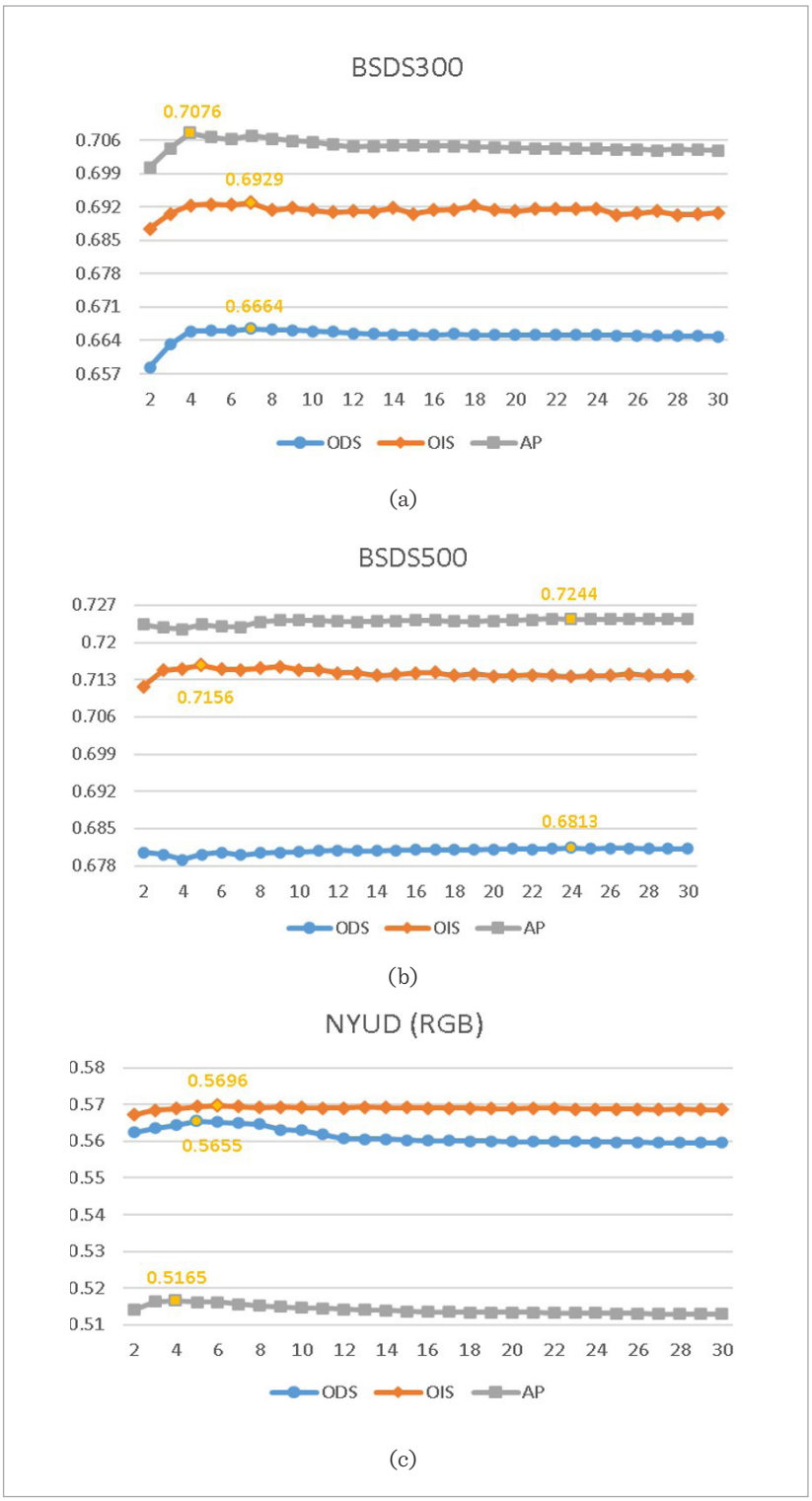

In Figure 8, function curve $A_t(t)$ illustrates the change in brightness, and the marked lines correspond to the optimal n values for different datasets. The theoretical-maximum-luminance is marked by the intersection of each marked line and the brightness curve, such that different theoretical-maximum-luminance are used to generate the theoretical-maximum-luminance image at different times. When t ≥ 200, the adaptation is considered complete, and the theoretical-maximum-luminance value is taken as 1.

The contour information obtained at different stages of adaptation are different. Therefore, we randomly select three different stages of information extraction in the adaptation process as an example. Figures 9b, 9c, and 9d depict the images corresponding to the time of adaptation t1, t2, and t3, respectively, whereas, 9f, 9g, and 9h represent the contour effect images extracted at the three adaptation times. The contour information in the image indicates the variability across the three selected moments, and the parts marked in red correspond to the focus of contour extraction at each adaptive moment.

4.2.1. BSDS Dataset Experiment

Tables 2-3 list the quantitative results of the DAC and other models tested on the BSDS dataset (BSDS300/500). In this experiment, we set σ =0.8, *ntheat* = 6, and *ws* = 5. We observe that the ODS of our model is 0.67, and the BSDS500 is 0.68. The DAC model only uses the V1 region. If SED only considers the information

Figure 8

Theoretical-maximum-luminance value at each adaptation stage and moment. BSDS300, BSDS500, NYUD datasets are represented by red, blue, and green, respectively. At(t) shows the change in brightness with respect to time. The intersection of each marked line and the brightness curve depicts the theoretical-maximum-luminance value at that moment

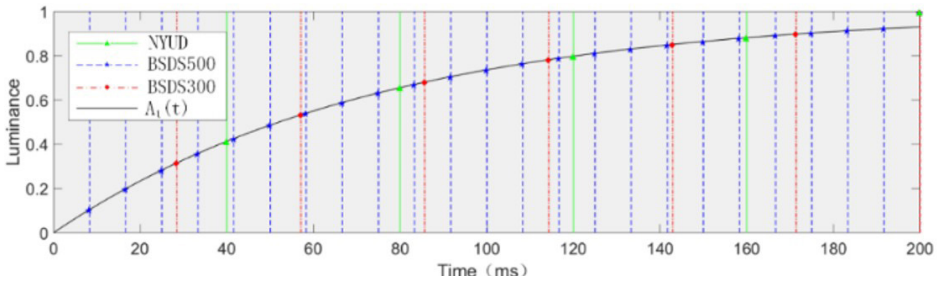

Figure 9

Information extraction stages in the adaptation process. (a) Original image; Images at times (b) t1, (c) t2, and (d) t3 during the adaptation process. (e)Ground truth; Information extraction at time (f) t1, (g) t2, and (h) t3 during the adaptation process. Red marks correspond to the focus of contour extraction at each adaptive moment

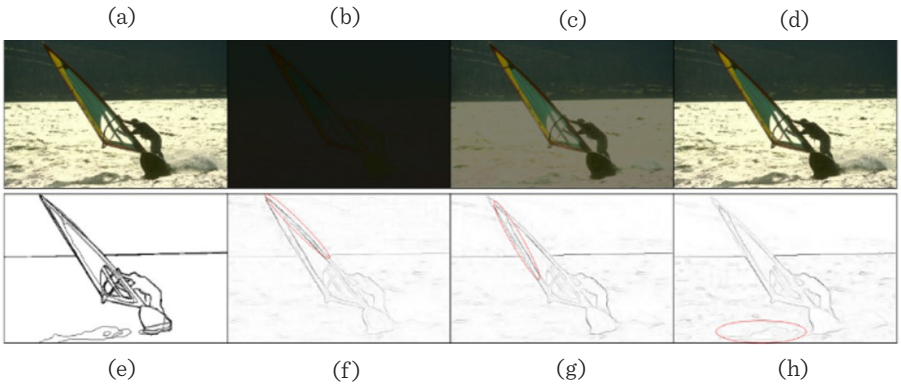

Table 2

Quantitative results for several contour detection models applied to color images of BSDS300/500

Model	BSDS 300		
	ODS	OIS	AP
CO [22]	0.64	0.66	0.64
SCO [24]	0.66	0.68	0.70
SED (only V1) [1]	0.66	0.70	0.70
Pb [28]	0.65	0.68	0.64
FDAG [19]	0.63	0.66	0.67
SCO+DL[11]	0.67	0.68	070
DAC	0.67	0.69	0.70

Table 3
Quantitative results for several contour detection models applied to color images of BSDS500

Model	BSDS 500		
	ODS	OIS	AP
CO [40]	0.65	0.68	0.65
SCO [41]	0.67	0.71	0.71
SED (only V1) [1]	0.67	0.71	0.70
Pb [28]	0.67	0.70	0.65
FDAG [6]	0.67	0.70	0.76
SCO+DL [15]	0.68	0.71	0.71
DAC	0.68	0.72	0.73

processing in the V1 region, the ODS of its experimental results is 0.66. The DAC model, therefore, has advantages over the SED (only V1) under the same conditions. Although the ODS of our model is the same as the SCO+DL, but there are still advantages over the other two parameters

To highlight the contribution of the visual adaptive processing model in information extraction, we randomly selected five images from the BSDS300/500 dataset for testing. The DAC model adds the DA model to the SCO model. Therefore, Figure 10 shows the comparison of the contour extraction performance of

Figure 10
Comparison of DA and SCO models. Red marks correspond to the detection effect better than SCO

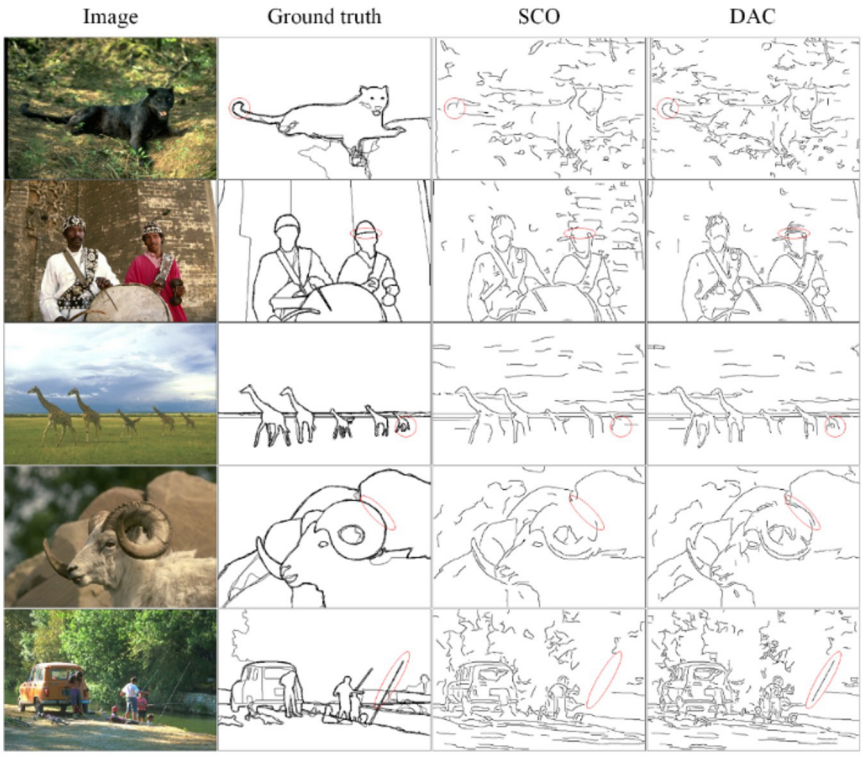

Figure 11
Quantitative comparison of several detection models on BSDS300 / 500

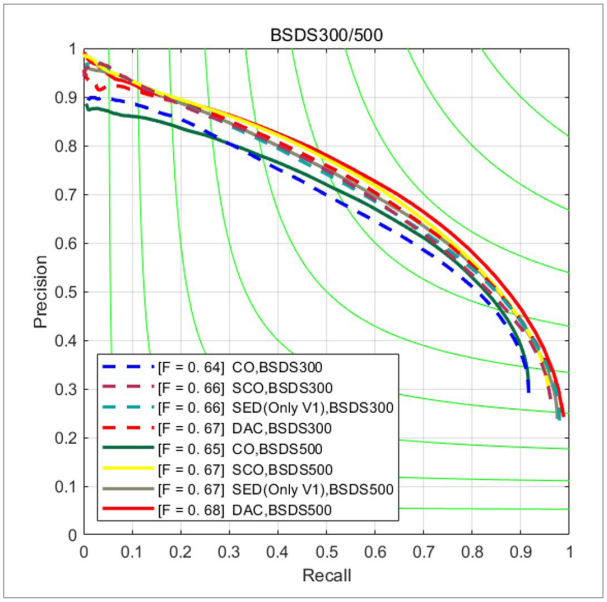

the DAC and the SCO models. The visual adaptation mechanism on the retina has a large effect on information extraction. Notably, the information obtained at different adaptation stages is different. Furthermore, detailed target information is obtained after integrating all the information. If only the original image is processed, some information may be lost, thereby reducing the accuracy of contour extraction. As indicated by the red marks on the image, the DAC model effectively extracts the contours that are similar in color and brightness, whereas the SCO model performs poorly Figure 11 shows the P-R curve of several bionic contour detection algorithms CO [40], SCO [41], SED (only V1) [1], and DAC on BSDS300/500.

Figure 11 compares the DAC model with that of the SCO model proposed by Yang and the Pb [28] model proposed by Martin et al. The results indicate that the DAC model performs well in information extraction.

To prove that the DA model has good robustness, and it can maintain great contour detection performance in dim visual scene, we perform gamma transforma-

Figure 12
Model comparison by experiment. The last column shows the F-measure for each model contour

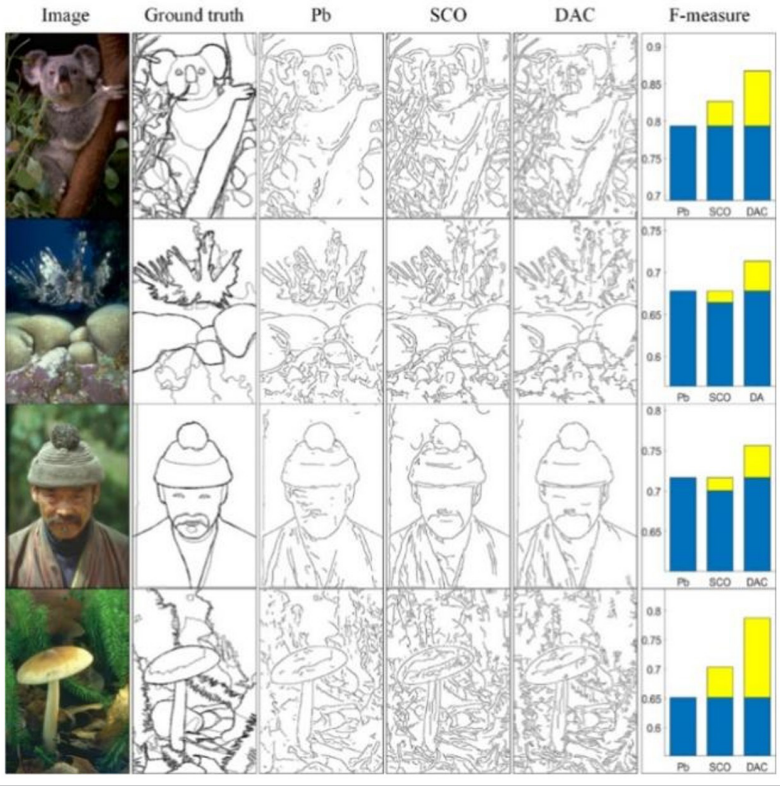

tion on all the images in the test data set. When the γ is greater than 1, It stretches areas of higher gray levels in the image, while compressing lower gray levels (reducing the contrast of the image to simulate a dim visual scene). In this work, we select the contour detection effect comparison of two images under different γ. The experimental results prove that when γ =2, the effect of the DAC model on the contour detection is significantly smaller than SCO model, and when the γ continues to increase, the image information is lost more seriously, which has a great impact on the result of contour detection. However, it can still be seen that the contour detection effect of the DAC model is superior to the SCO model.

We select the contour extraction effect of the two images under different γ for analysis. As can be seen from Figure 13, the blue marked area of the first image (the contour area of the reflection in the water surface) DAC model is better than the SCO model in retention effect of the contour when the a continues to increase. In the second image, the blue marked area (the non-contour area of the background in the image) DAC model is significantly better than the SCO model in the suppression effect of non-contour when the γ continues to increase. In summary, the DAC model proposed in this paper has great robustness and it can extract relatively good target contours in a dim environment.

4.2.2. NYUD Data Set Experiment

To better demonstrate the advantages of the DAC model, we conducted additional verification experiments on the NYUD dataset. In this experiment, we set σ =1.2, *ntheat* = 6, and *ws*=5. The NUYD dataset comprises RGB images and HHA depth images. Therefore, the results obtained were as follows: NYUD-RGB image processing results, NYUD-HHA image processing results, and NYUD-RGB-HHA image processing results, which are obtained by combining the first two sets of results. Figure 14 depicts that the P-R curves of several bionic contour detection models in RGB, HHA, and RGN-HHA respectively, including CO [40], SCO [41], SED (Only V1) [1], and DAC.

The contour extraction performance of the same model varies depending on the dataset used. From the results obtained on the BSDS300 / 500 and NYUD datasets, it can be concluded that the DA model exhibits great generality. In comparison with the other models, the detection effect in the case of the NYUD dataset is more reliable, as the indoor lighting is dim compared to outdoor

Figure 13

Comparison of DAC model and SCO model under different γ. In each image, the top is the SCO model, and the bottom is the DAC model. In the Ground truth, the red mark indicates the area we selected for comparison, and the blue marked area indicates the influence on the contour detection effect of the DAC model and the SCO model as the γ changes

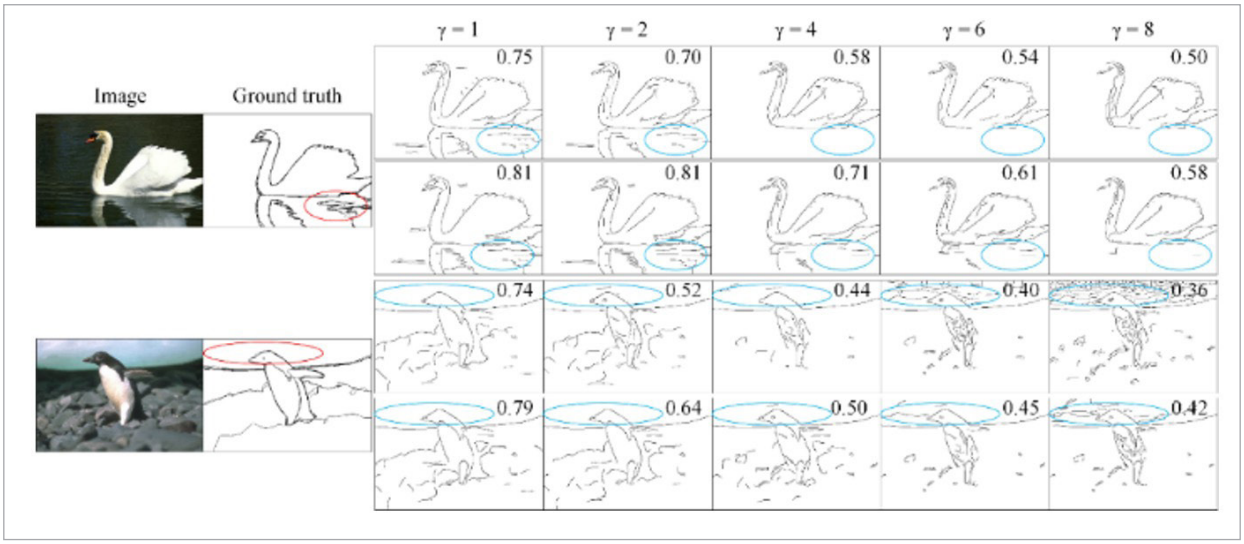

Figure 14
Quantitative comparison of several detection models on NYUD dataset

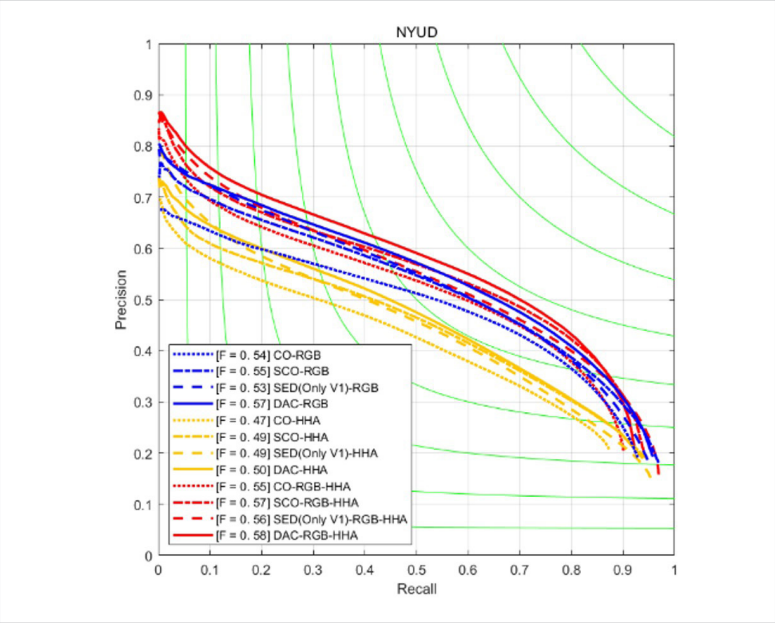

Figure 15
Comparison between DAC model and SCO model

lighting. Using the DAC model to integrate the extracted information therefore yields better performance in the extraction of darker edges of the indoor scene, as indicated by the red box in Figure 15.

5. Bionic Mechanism Combined with Deep Learning

Inspired by ConvNets using biologically inspired mechanisms for convolutional neural networks [16]. To discuss the possibility of combining bionics and deep learning methods, this paper fuses the proposed methods with deep learning models. Our method has some changes to the original image, it plays a significant role in texture suppression and detail extraction. Therefore, I think that fusing our method with the deep learning model has certain research significance. Thus, we use the adaptive image as a new feature, and combine the original RGB image as the input of the convolutional neural network. Table 4 shows the quantitative results of our method combined with the deep learning model and compared with the original deep learning model. In this experiment, we use the enhanced data of BSDS500 and the flipped PASCAL VOC context data set [23] as training data. The original HED [39] has only single-scale results, so that HED+DA is also single-scale results in the table, and the others are multi-scale. Furthermore, ODS and OIS are usually related to the performance evaluation of edge detection, while AP is more commonly used in object detection or classification tasks. This task places greater emphasis on the continuity and accura-

cy of the edges, therefore AP is only used as a reference value. The results of the DA model imported into the CED preprocessing network will have a certain impact on the overall quality of the image, which actually indirectly improves the robustness of the model. Therefore, the AP value will decrease to some extent.

Table 4
The comparison on BSDS500 dataset

Model	BSDS 500		
	ODS	OIS	AP
HED [39]	.788	.808	.840
RCF [19]	.811	.830	.846
CED [34]	.815	.833	.889
LRC [17]	.816	.836	.864
HED+DA	.799	.817	.833
RCF+DA	.813	.832	.856
CED+DA	.816	.834	.869
LRC+DA	.817	.840	.868

6. Discussion and Conclusions

Contour detection is usually performed in two steps; first, the target information is extracted, and then, the texture information is suppressed. Various physiological mechanism-based models have been proposed and effectively applied to numerous image processing tasks. To extract target information, a model based on visual adaptation of the retina is proposed in this study. This model is capable of extracting a large amount target information even in complex scenes.

The main contribution of this study can be summarized as follows. the process of information extraction in humans must be a gradual one, and the information presented to the mind at different visualization stages must also be different. Unlike in previous studies, before the information processing step, we added a visual gradient processing step to simulate the gradient of the image. Therefore, we obtainedpieces of image information at different visual adaptation periods, which are then integrated to yield a relatively more complete target image information.

The dark adaptation vision model proposed in this paper was quantitatively tested on the RuG, BSDS, and NYUD datasets. In comparison with the current bionic contour detection model, the DA model can extract more contour information from complex scenes. And discussed the possibility of combining the bionic model and the deep learning model. From the results, it can be seen that the combination of the two can improve the extraction of the target contour to a certain extent. However, the human visual adaptation system is highly complicated, as it not only adapts the brightness, but also the color. Hence, the DA model is incomplete in that regard. The model proposed in this study only uses the retina, LGN, and primary visual cortex to process the image, and does not apply to the higher visual cortex. Studies have shown that the adaptation of one eye to strong colored lights affects the color vision of the other eye, which indicates that color adaptation can only be performed by advanced visual systems. Thus, the future research must focus on studying how the higher-level visual cortex processes color adaptation on the basis of preprocessing can be performed. In summary, the theoretically complete visual adaptation process should include brightness and color adaptations, which are closely related to one another and form a closed loop. The color adaptation information should be returned from the advanced visual cortex to the primary visual cortex through feedback and the preceding brightness adaptation information. This combination is expected to form a completely closed information processing loop.

Acknowledgement

The authors appreciate the anonymous reviewers for their helpful and constructive comments on an earlier draft of this paper. This work was supported by China University Industry University Research Innovation Fund-New Generation Information Tech-nology Innovation Project Topic (Grant (2021ITA11001).

References

1. Akbarinia, A., Parraga, C. A. Feedback and Surround Modulated Boundary Detection. International Journal of Computer Vision, 2018, 126(12), 1367-1380. https://doi.org/10.1007/s11263-017-1035-5
2. Azzopardi, G., Petkov, N. A CORF Computational Model of a Simple Cell That Relies on LGN Input Outperforms the Gabor Function Model. Biological Cybernetics, 2012, 106, 177-189. https://doi.org/10.1007/s00422-012-0486-6

3. Azzopardi, G., Rodríguez-Sánchez, A., Piater, J., Petkov, N. A Push-Pull CORF Model of a Simple Cell with Antiphase Inhibition Improves SNR and Contour Detection. PLoS One, 2014, 9(7), e98424. https://doi.org/10.1371/journal.pone.0098424
4. Bao, P., Zhang, L., Wu, X. Canny Edge Detection Enhancement by Scale Multiplication. IEEE Transactions on Pattern Analysis and Machine Intelligence, 2005, 27(9), 1485-1490. https://doi.org/10.1109/TPAMI.2005.192
5. Cao, Y.-J., Lin, C., Pan, Y.-J., Zhao, H.-J. Application of the Center-Surround Mechanism to Contour Detection. Multimedia Tools and Applications, 2019, 78, 25121-25141. https://doi.org/10.1007/s11042-018-6924-2
6. Daugman, J. G. Uncertainty Relation for Resolution in Space, Spatial Frequency, and Orientation Optimized by Two-Dimensional Visual Cortical Filters. JOSA A, 1985, 2(7), 1160-1169. https://doi.org/10.1364/JOSAA.2.001160
7. Dowling, J. E. The Retina: An Approachable Part of the Brain. Harvard University Press, 1987. ISBN: 9780674766800
8. Grigorescu, C., Petkov, N., Westenberg, M. A. Contour Detection Based on Nonclassical Receptive Field Inhibition. IEEE Transactions on Image Processing, 2003, 12(7), 729-739. https://doi.org/10.1109/TIP.2003.814250
9. Hecht, S., Haig, C., Chase, A. M. The Influence of Light Adaptation on Subsequent Dark Adaptation of the Eye. The Journal of General Physiology, 1937, 20(6), 831-850. https://doi.org/10.1085/jgp.20.6.831
10. Isola, P., Zoran, D., Krishnan, D., Adelson, E. H. Crisp Boundary Detection Using Pointwise Mutual Information. In Computer Vision-ECCV 2014: 13th European Conference, Zurich, Switzerland, September 6-12, 2014, Proceedings, Part III 13, Springer, 2014, 799-814. https://doi.org/10.1007/978-3-319-10578-9_52
11. Kazakova, N., Margala, M., Durdle, N. G. Sobel Edge Detection Processor for a Real-Time Volume Rendering System. In 2004 IEEE International Symposium on Circuits and Systems, IEEE, 2004, 2, II-913. https://doi.org/10.1109/ISCAS.2004.1328866
12. La Cara, G.-E., Ursi, M. A Model of Contour Extraction Including Multiple Scales, Flexible Inhibition, and Attention. Neural Networks, 2008, 21(5), 759-773. https://doi.org/10.1016/j.neunet.2008.04.003
13. Ledda, P., Santos, L. P., Chalmers, A. A Local Model of Eye Adaptation for High Dynamic Range Images. In Proceedings of the 3rd International Conference on Computer Graphics, Virtual Reality, Visualization and Interaction in Africa, 2004, 151-160. https://doi.org/10.1145/1029949.1029974
14. Leibrock, C. S., Reuter, T., Lamb, T. D. Molecular Basis of Dark Adaptation in Rod Photoreceptors. Eye, 1998, 12(3), 511-520. https://doi.org/10.1038/eye.1998.144
15. Li, F., Lin, C., Zhang, Q., Wang, R. A Biologically Inspired Contour Detection Model Based on Multiple Visual Channels and Multi-Hierarchical Visual Information. IEEE Access, 2020, 8, 15410-15422. https://doi.org/10.1109/ACCESS.2020.2966916
16. Liang, Z., Shen, W., Shou, T. Enhancement of Oblique Effect in the Cat's Primary Visual Cortex via Orientation Preference Shifting Induced by Excitatory Feedback from Higher-Order Cortical Area21a. Neuroscience, 2007, 145(1), 377-383. https://doi.org/10.1016/j.neuroscience.2006.12.046
17. Lin, C., Cui, L., Li, F., Cao, Y. Lateral Refinement Network for Contour Detection. Neurocomputing, 2020, 409, 361-371. https://doi.org/10.1016/j.neucom.2020.05.073
18. Lin, C., Xu, G., Cao, Y. Contour Detection Model Using Linear and Non-Linear Modulation Based on Non-CRF Suppression. IET Image Processing, 2018, 12(6), 993-1003. https://doi.org/10.1049/iet-ipr.2017.0679
19. Liu, Y., Cheng, M.-M., Hu, X., Wang, K., Bai, X. Richer Convolutional Features for Edge Detection. In Proceedings of the IEEE Conference on Computer Vision and Pattern Recognition, 2017, 3000-3009. https://doi.org/10.1109/CVPR.2017.656
20. Maninis, K.-K., Pont-Tuset, J., Arbeláez, P., Van Gool, L. Convolutional Oriented Boundaries: From Image Segmentation to High-Level Tasks. IEEE Transactions on Pattern Analysis and Machine Intelligence, 2017, 40(4), 819-833. https://doi.org/10.1109/TPAMI.2017.2700300
21. Martin, D. R., Fowlkes, C. C., Malik, J. Learning to Detect Natural Image Boundaries Using Local Brightness, Color, and Texture Cues. IEEE Transactions on Pattern Analysis and Machine Intelligence, 2004, 26(5), 530-5494. https://doi.org/10.1109/TPAMI.2004.1273918
22. Melotti, D., Heimbach, K., Rodríguez-Sánchez, A., Strisciuglio, N., Azzopardi, G. A Robust Contour Detection Operator with Combined Push-Pull Inhibition and Surround Suppression. Information Sciences, 2020, 524, 229-240. https://doi.org/10.1016/j.ins.2020.03.081
23. Mottaghi, R., Chen, X., Liu, X., Cho, N.-G., Lee, S.-W., Fidler, S. The Role of Context for Object Detection and Semantic Segmentation in the Wild. In Proceedings of the IEEE Conference on Computer Vision and Pattern Recognition, 2014, 891-898. https://doi.org/10.1109/CVPR.2014.119
24. Olson, C. F., Huttenlocher, D. P. Automatic Target Recognition by Matching Oriented Edge Pixels. IEEE

Transactions on Image Processing, 1997, 6(1), 103-113. https://doi.org/10.1109/83.552100

25. Papari, G., Petkov, N. Edge and Line Oriented Contour Detection: State of the Art. Image and Vision Computing, 2011, 29(2-3), 79-103. https://doi.org/10.1016/j.imavis.2010.08.009
26. Pattanaik, S. N., Tumblin, J., Yee, H., Greenberg, D. P. Time-Dependent Visual Adaptation for Fast Realistic Image Display. In Proceedings of the 27th Annual Conference on Computer Graphics and Interactive Techniques, 2000, 47-54. https://doi.org/10.1145/344779.344810
27. Shlaer, S. The Relation Between Visual Acuity and Illumination. The Journal of General Physiology, 1937, 21(2), 165-188. https://doi.org/10.1085/jgp.21.2.165
28. Spratling, M. W. Image Segmentation Using a Sparse Coding Model of Cortical Area V1. IEEE Transactions on Image Processing, 2012, 22(4), 1631-1643. https://doi.org/10.1109/TIP.2012.2235850
29. Staddon, J. E. R. Adaptive Behavior and Learning. Cambridge University Press, 2016. https://doi.org/10.1017/CBO9781139998369
30. Strisciuglio, N., Azzopardi, G., Petkov, N. Robust Inhibition-Augmented Operator for Delineation of Curvilinear Structures. IEEE Transactions on Image Processing, 2019, 28(12), 5852-5866. https://doi.org/10.1109/TIP.2019.2922096
31. Strisciuglio, N., Lopez-Antequera, M., Petkov, N. Enhanced Robustness of Convolutional Networks with a Push-Pull Inhibition Layer. Neural Computing Applications, 2020. https://doi.org/10.1007/s00521-020-04751-8
32. Tabb, M., Ahuja, N. Multiscale Image Segmentation by Integrated Edge and Region Detection. IEEE Transactions on Image Processing, 1997, 6(5), 642-655. https://doi.org/10.1109/83.568922
33. Van Vliet, L. J., Young, I. T., Beckers, G. L. An Edge Detection Model Based on Non-Linear Laplace Filtering. In Machine Intelligence and Pattern Recognition, Elsevier, 1988, 7, 63-73. https://doi.org/10.1016/B978-0-444-87137-4.50011-4
34. Wang, Y., Zhao, X., Huang, K. Deep Crisp Boundaries. In Proceedings of the IEEE Conference on Computer Vision and Pattern Recognition, 2017, 3892-3900. https://doi.org/10.1109/CVPR.2017.414
35. Wei, H., Dai, Z.-L., Zuo, Q.-S. A Ganglion-Cell-Based Primary Image Representation Method and Its Contribution to Object Recognition. Connection Science, 2016, 28(4), 311-331. https://doi.org/10.1080/09540091.2016.1212813
36. Wei, H., Lang, B., Zuo, Q. Contour Detection Model with Multi-Scale Integration Based on Non-Classical Receptive Field. Neurocomputing, 2013, 103, 247-262. https://doi.org/10.1016/j.neucom.2012.10.009
37. Wei, Y., Xia, W., Lin, M., Huang, J., Ni, B., Dong, J. HCP: A Flexible CNN Framework for Multi-Label Image Classification. IEEE Transactions on Pattern Analysis and Machine Intelligence, 2015, 38(9), 1901-1907. https://doi.org/10.1109/TPAMI.2015.2491929
38. Xiao, J., Cai, C. Contour Detection Based on Horizontal Interactions in Primary Visual Cortex. Electronics Letters, 2014, 50(5), 359-361. https://doi.org/10.1049/el.2014.0298
39. Xie, S., Tu, Z. Holistically-Nested Edge Detection. In Proceedings of the IEEE International Conference on Computer Vision, 2015, 1395-1403. https://doi.org/10.1109/ICCV.2015.164
40. Yang, K., Gao, S., Li, C. Efficient Color Boundary Detection with Color-Opponent Mechanisms. In Proceedings of the IEEE Conference on Computer Vision and Pattern Recognition, 2013, 2810-2817. https://doi.org/10.1109/CVPR.2013.361
41. Yang, K.-F., Gao, S.-B., Guo, C.-F., Li, C.-Y., Li, Y.-J. Boundary Detection Using Double-Opponency and Spatial Sparseness Constraint. IEEE Transactions on Image Processing, 2015, 24(8), 2565-2578. https://doi.org/10.1109/TIP.2015.2425538
42. Yang, K.-F., Li, C.-Y., Li, Y.-J. Multifeature-Based Surround Inhibition Improves Contour Detection in Natural Images. IEEE Transactions on Image Processing, 2014, 23(12), 5020-5032. https://doi.org/10.1109/TIP.2014.2361210
43. Zeng, C., Li, Y., Li, C. Center-Surround Interaction with Adaptive Inhibition: A Computational Model for Contour Detection. NeuroImage, 2011, 55(1), 49-66. https://doi.org/10.1016/j.neuroimage.2010.11.060
44. Zeng, C., Li, Y., Yang, K., Li, C. Contour Detection Based on a Non-Classical Receptive Field Model with Butterfly-Shaped Inhibition Subregions. Neurocomputing, 2011, 74(10), 1527-1534. https://doi.org/10.1016/j.neucom.2010.05.014
45. Zhang, J., Barhomi, Y., Serre, T. A New Biologically Inspired Color Image Descriptor. In Computer Vision-ECCV 2012: 12th European Conference on Computer Vision, Florence, Italy, October 7-13, 2012, Proceedings, Part V 12, Springer, 2012, 312-324. https://doi.org/10.1007/978-3-642-33715-4_23
46. Zhao, D., Yang, L., Wu, X., Wang, N., Li, H. An Improved Roberts Edge Detection Algorithm Based on Mean Filter and Wavelet Denoising. In Advances in Information Technology and Industry Applications, Springer, 2012, 299-305. https://doi.org/10.1007/978-3-642-26001-8_39